Electrochimica Acta 456 (2023) 142437

Contents lists available at ScienceDirect

Electrochimica Acta

journal homepage: www.journals.elsevier.com/electrochimica-acta

Design considerations and cycling guidance for aluminum foil anodes in lithium-ion rechargeable cells

Jia Zhang [a], Tianye Zheng [a,b,*], Kwok-ho Lam [a,c], Steven T. Boles [d,*]

[a] Department of Electrical Engineering, The Hong Kong Polytechnic University, Hung Hom, Kowloon, Hong Kong
[b] Photonics Research Institute, The Hong Kong Polytechnic University, Hung Hom, Kowloon, Hong Kong
[c] Centre for Medical and Industrial Ultrasonics, James Watt School of Engineering, University of Glasgow, Glasgow, Scotland, United Kingdom
[d] Department of Energy and Process Engineering, Faculty of Engineering, Norwegian University of Science and Technology (NTNU), Trondheim, Norway

ARTICLE INFO

Keywords:
Al foil anodes
Prelithiation
β-LiAl
Kinetics
Cyclability

ABSTRACT

Al foil is an attractive anode candidate for Li-ion rechargeable batteries, but the systemic problem of fast capacity degradation limits its re-introduction in practical applications. Partial lithiation-delithiation does mitigate the issue to a certain degree, but the cycle life is still tied to the problems associated with the phase transformation between β-LiAl and α-Al. Utilizing the solubility range of β-LiAl has been proven to be a feasible approach to stabilize the β-LiAl grown on an Al foil, i.e., the β-LiAl(Al) anode, but the electrochemically driven ion transport limitations of this electrode remain largely unclear. Herein, we present comprehensive electrochemical analyses of the β-LiAl(Al) electrode to shed light on its kinetic limitations which have intrinsic links to the electrode thickness and total cell capacity. Results show that the β-LiAl(Al) electrode can be charged at a C-rate as high as 2.9 C when a proper prelithiation is done for an Al foil. The superior rate capability is suggested to partly originate from the fast lithium diffusion in β-LiAl: ~10^{-7} $cm^2 \cdot s^{-1}$ at room temperature. Furthermore, the cells consisting of β-LiAl(Al) vs. commercial $Li_4Ti_5O_{12}$ exhibit promising cycling performances, even at 10 $mA \cdot cm^{-2}$, giving 300 cycles with a capacity retention of ~80%. With a systematic investigation of the limiting mechanisms focusing on correlating the prelithiation depth and the cycle life, the cyclability of the β-LiAl(Al) electrode at different current densities (0.5–10 $mA \cdot cm^{-2}$) is mapped out, providing comprehensive guidance for the practical utilization of the β-LiAl(Al) anode in a range of Li-ion cell types, from all-solid-state batteries to hybrid capacitors.

1. Introduction

Metallic foil anodes have long attracted researchers' attention in lithium rechargeable batteries since the early 1970s when Rao et al. demonstrated that the lithium-aluminum anode can effectively suppress Li dendrite formation [1]. However, the disappointing cycle life for Al or other metal-based anodes (e.g., Li_xSn, Li_xSb, Li_xBi [2]) generally quelled the pursuit of solving such issues, in light of the commercialization of graphite anode in Li-ion battery (LIB) in the early 1990s and the powder slurry-coating technique [3] which mirrors that used for the cathode. Recently, there is a reignited interest in foil-type alloy anodes because of their prospects for sustainability, lower manufacturing costs, and high specific capacities [4], compared to nanostructured composite electrodes. Among all the potential elemental foils, Sn, Al, and In are highlighted as the most promising anode candidates for LIB [4]. From the application perspective, Al foil is more attractive than the others considering its high specific capacity (993 $mAh \cdot g^{-1}$ for LiAl and 1152 $mAh \cdot g^{-1}$ for $Li_{1.16}Al$ [5]), rich abundance (the second most abundant metal), low cost (mass-produced), and moderate volume expansion (~95% for the α-Al to β-LiAl phase transformation [6,7]). However, the poor cycling issue of Al foil electrodes remains unresolved.

The reason why Al anodes can only be cycled a dozen times has been attributed to a number of things over the years, including Li trapping during cycling [8], secondary SEI formation on the fresh surfaces at crack regions [9], and delithiation-induced formation of nanopores [10]. Although a prelithiation step has been employed to improve the electrochemical performance of some alloy-type anodes [11–13], the cycle life of prelithiated Al remains unsatisfactory and perplexing. An

* Corresponding authors at: Department of Energy and Process Engineering, Faculty of Engineering, Norwegian University of Science and Technology (NTNU), Trondheim, Norway.
E-mail addresses: darren.ty.zheng@connect.polyu.hk (T. Zheng), steven.boles@ntnu.no (S.T. Boles).

https://doi.org/10.1016/j.electacta.2023.142437
Received 15 January 2023; Received in revised form 17 April 2023; Accepted 17 April 2023
Available online 18 April 2023

early study found that the capacity of a β-LiAl(Al)//LFP full cell decays after about 10 cycles [14]. Similar results are observed in recent studies on prelithiated Al foil anode: for instance, Yu et al. reported that the mechanically prelithiated Al foil shows a high initial coulombic coefficiency of ~90% in a full cell, but the cycling stability collapses after 40 cycles [15]. Crowley et al. observed Li_3Al_{97} foil undergoes dramatic capacity decay from the first few cycles [16]. Benchmarking efforts have also been put into understanding the degradation behavior of Al foil anodes [17]. With the cyclability for β-LiAl(Al) at the present level still far below cycling requirements, viable strategies are required to prolong the lifetime of the β-LiAl(Al) anode. Recently, Li et al. reported that uniting the lithiation direction of Al foil anodes could largely circumvent the mechanical strain induced by the volume expansion, thereby enhancing the anode cyclability (i.e., the reversibility of α/β phase transformations) [18]. Alternatively, restricting the β to α phase transformations is proved to be effective to prolong the cycle life of the Al foil anode, considering that there exists a Li solubility range in β-LiAl at room temperature, corresponding to the Li content from ca. 47.8 at% to 53.7 at%. Owing to a capacity of -242 $mAh{\cdot}g^{-1}$, normalized to Al, utilizing this solubility range of β-LiAl can be a viable strategy to stabilize Al anodes in LIB applications. This was verified by the long-term cycling stability of the β-LiAl(Al) anode with merely -4% capacity decay after 500 cycles in a full cell [5]. However, to our knowledge, no systematic investigation has been done on this β-LiAl solubility range regarding the cyclability and the rate capability.

The physio-chemical properties, such as decent electronic and ionic conductivities [19,20], could potentially make the β-LiAl highly rate capable. However, the dense structure of metallic foil will invariably provide a kinetic barrier to the lithium transport, limiting the discharge/charge rate to some extent. Therefore, to understand the kinetic limitation imposed by the electrode design and material, interpreting the Li diffusion behavior in β-LiAl is of vital importance. Much of the early literature shed light on the Li diffusivity in β-LiAl at elevated temperatures (e.g., 200 °C [21], 485 K [22], 415 °C [23,24], 600 °C [23,25]) by using nuclear magnetic resonance (NMR) and electrochemical techniques, such as the galvanostatic or potentiostatic intermittent titration (GITT or PITT), and electrochemical impedance spectroscopy (EIS) techniques. The Li diffusivities were determined to range from 10^{-5} to 10^{-6} $cm^2{\cdot}s^{-1}$, but the information at room temperature can hardly be found, except those published almost 40 years ago [26].

In this work, we conduct systematic investigations on the cyclability of the β-LiAl(Al) electrode at various rates and quantitively explore the Li diffusion behavior using electrochemical techniques at room temperature, such that new understandings for the interplay between the rate capability and diffusion kinetics of β-LiAl can be expected. The long-term cycling of β-LiAl(Al) electrode is also extensively investigated in LTO//β-LiAl(Al) cells at a current density ranging from 0.5 to 10 $mA{\cdot}cm^{-2}$. The established cyclability mapping provides comprehensive guidance for the practical use of the β-LiAl(Al) electrodes in any lithium-ion cell, including rechargeable batteries and hybrid capacitive devices.

2. Material and methods

All the electrochemical measurements, e.g., chronoamperometry (CA), galvanostatic charge-discharge (GCD), electrochemical impedance spectra (EIS), are conducted using a VMP 300 potentiostat (Biologic Technologies, France) and LAND battery testing system at room temperature. The materials used in this work include: Al foil (99.7%, 180 μm-thick, Toyo Aluminium K.K.) as the precursor for the working electrode, Li foil as the counter electrode, $Li_4Ti_5O_{12}$ cathode (LTO, 1.25 $mAh{\cdot}cm^{-2}$, NEI corporation), 1 M $LiPF_6$ in EC:EMC 3:7 vol% electrolyte (DoDoChem, China), glass fiber separator (Whatman®), Celgard® 2400 separator, 2025-type coin cell components (cases, spacers, springs).

2.1. Preparation of β-LiAl(Al) electrode

The β-LiAl on Al foil bilayer electrode (β-LiAl as active material, Al as current collector) was prepared by an electrochemical prelithiation on Al foil in Al//Li half cells using the CA technique. Firstly, the half cell was held at 400 mV versus Li/Li^+ for 4 h to largely isolate the irreversible surface reactions. Then the potential decreases to 10 mV vs. Li/Li^+, followed by a 10-minute hold at the same potential to form a large number of β-LiAl nuclei on the electrode surface [26]. Finally, the potential was adjusted to a higher level at 200 mV vs. Li/Li^+ to enable the phase propagation until the desired capacity, e.g., ca. 3.05 mAh for 10 μm thick nominal prelithiation depth (10 μm Al prelithiated to β-LiAl, the remaining 170 μm-thick Al as the current collector), which is abbreviated as P-Al-10. Accordingly, the P-Al-20, P-Al-80, and P-Al-100 denote the prelithiated Al foil with nominal prelithiation depths of 20, 80, and 100 μm, respectively.

2.2. Electrode characterizations

X-ray diffraction (XRD) tests were performed on the β-LiAl(Al) electrode that was collected by disassembling the Al//Li half-cell in an Ar-filled glovebox after going through the prelithiation protocol. A Rigaku SmartLab 9 kW X-ray diffractometer with Cu Kα radiation was employed using a scan speed of 5 $^\circ{\cdot}min^{-1}$ in a 2θ angle range from 20 to 80°

Electrochemical impedance spectroscopy (EIS) was carried out on the samples of P-Al-10 to P-Al-100, prepared by the galvanostatic charge-discharge sequence in Section 2.3 on the same Al foil, with 10 mV perturbation amplitude in the frequency ranging from 100 kHz to 10 mHz at room temperature.

2.3. Galvanostatic charge-discharge (GCD) sequences

Galvanostatic techniques were performed on the β-LiAl(Al) electrodes in half cells to systematically explore the electrochemical performances (an example at 1.0 C is shown in Fig. 1a,b). The P-Al-10 electrode was initially delithiated to 0.405 V (before the delithiation plateau potential, Fig. 1c) at a constant current of 0.073 mA to desaturate the β-LiAl phase (Li-poor, Fig. 1b). The 0.073 mA is equivalent to 0.1 C for P-Al-10, based on the theoretical capacity of the β-LiAl solubility range (242 $mAh{\cdot}g^{-1}$-Al [5]). Afterward, the electrode underwent a lithiation at various C-rates to saturate the β-LiAl layer to form Li-rich β-LiAl, and subsequently move the phase boundary to reach a 20 μm-thick nominal prelithiation depth (i.e., P-Al-20). Lastly, this designated delithiation-lithiation process was repeated 9 times for the same Al disk until reaching the 100 μm-thick nominal prelithiation depth (i.e., P-Al-100). The detailed schematic illustration for the above-mentioned galvanostatic de-/lithiation sequences is shown in Fig. 1d. The capacity difference between the Li-poor and the Li-rich β-LiAl is considered as the capacity that is solely contributed by the solubility range. Thereby, the capacities of P-Al-10 to P-Al-100 within the solubility range at different C-rates (corresponding current details in Table S1) could be all collected using the above-mentioned methods. Importantly, it can be noted that the reverse transformation of β-LiAl to α-Al is never enacted with this protocol, thus ensuring the β-LiAl phase integrity and only the forward propagation (i.e., consumption of α-Al).

2.4. Galvanostatic intermittent titration technique (GITT)

To explore the Li diffusivity in β-LiAl, GITT was performed on the β-LiAl(Al) electrodes in half cells at room temperature. Specifically, a current pulse was applied for a defined period τ (3 min), followed by a long relaxation (5 h) to ensure that the electrode reaches its equilibrium state (Fig. S1). The equilibrium potentials (E_s) after each pulse were recorded. The upper potential limit for the GITT measurement was set at 0.41 V vs. Li/Li^+ to largely minimize the phase boundary movement

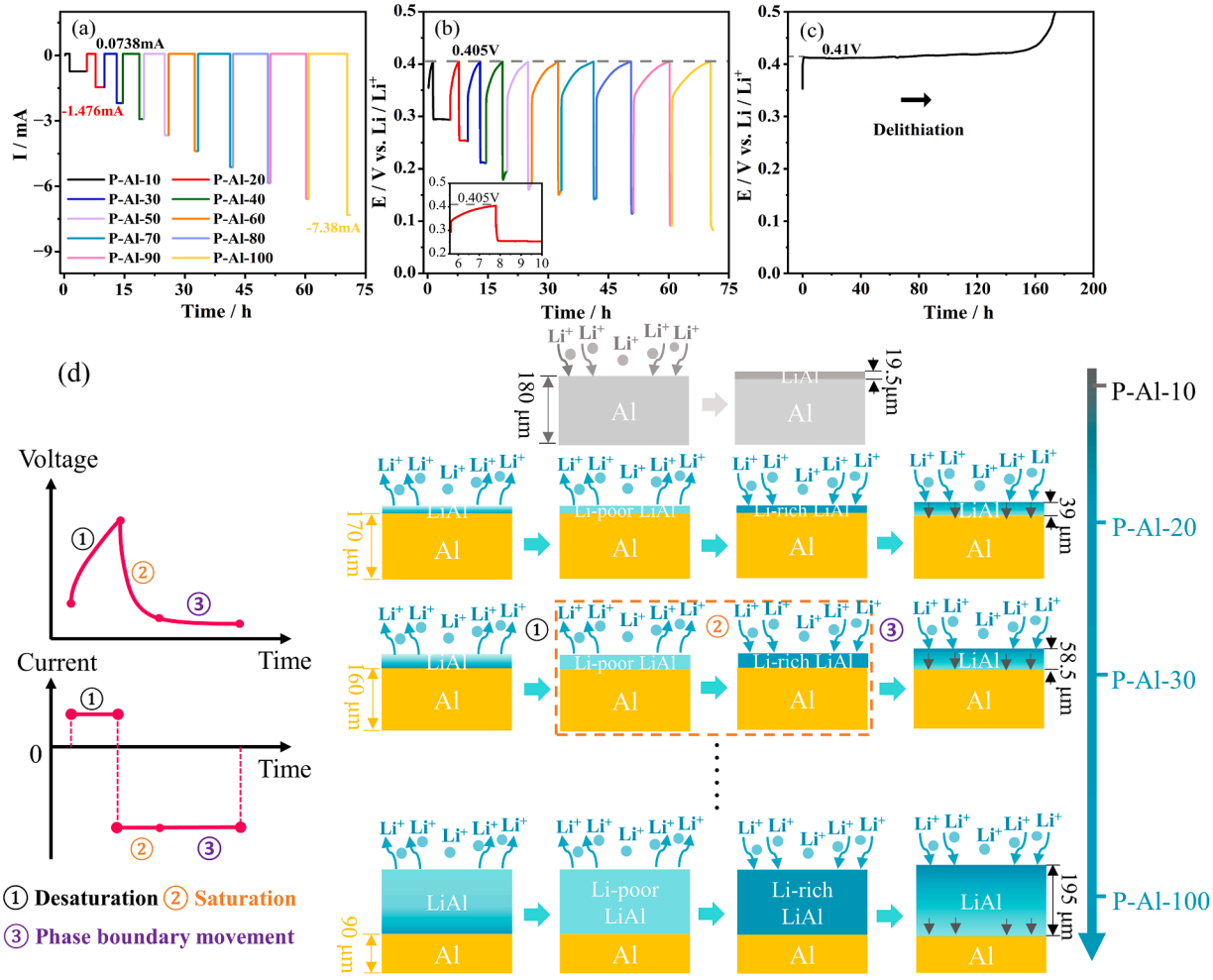

Fig. 1. An example of a full GCD sequence at 1.0 C: (a) Current-time profile and (b) Voltage-time profile. (c) Galvanostatic delithiation curve under 0.073 mA (0.1 C for P-Al-10). The delithiation plateau is at around 0.41 V. (d) Schematic illustrations of the GCD sequence.

(Fig. 1c). In this case, the Li diffusivity in β-LiAl can be calculated by Eq. (1) [23]:

$$D_{Li} = \frac{4L^2}{\pi\tau}\left(\frac{\Delta E_s}{\Delta E_\tau}\right)^2 \quad (\tau << L^2/D) \tag{1}$$

Where L denotes the thickness of the β-LiAl layer, τ is the pulse time. As for ΔE_sandΔE_τ, the former is the difference between the equilibrium potentials obtained from two contiguous relaxations while the latter is the potential change within each pulse. The GITT was stopped when the cell potential reaches ca. 0.41 V vs. Li/Li^+. We reasonably assume that the β-LiAl(Al) electrode after the last titration reaches the Li-poor β-LiAl phase ($Li_{0.916}Al$ [5]) and the Li stoichiometry x in Li_xAl in former titration can be deduced from: $x = 0.916 + n\delta$. Here, n is the pulse number counted reversely from the final pulse, and δ is the Li concentration change caused by each small current pulse, which can be estimated by: $\delta = \frac{I\tau M}{zmF}$($z$ is the electron number during the electrochemical reaction, F is the Faraday constant, m and M are the weight and the molar mass of Al, respectively).

2.5. Mapping for cyclability of β-LiAl(Al) electrodes

The long-term cycling and rate performance of β-LiAl(Al) electrodes were examined at various current densities in LTO//β-LiAl(Al) cells with Celgard 2400 as the separator and 1 M $LiPF_6$ in EC:EMC 3:7 vol% as the electrolyte. A mapping of the cyclability of LTO//β-LiAl(Al) cells is created with 5 rows and 5 columns. The detailed information on the prelithiation depth of the electrodes, the working voltage windows, and the current densities are summarized in Table S2.

3. Results

3.1. Electrode characterizations

Fig. 2a shows the X-ray diffractograms of the P-Al-100 electrode, with the macroscopic views of both the front and the back side presented in Fig. 2b. From the diffractograms, typical peaks for crystalline β-LiAl (cubic, PDF: JCPDS 03–1215, lattice constant: $a = 0.6373$ nm), and α-Al phase (fcc, PDF: JCPDS 04–0787) are observed in the front side of the P-Al-100 electrode. Other crystalline Li-Al intermetallic compounds, such as Li_3Al_2, $Li_{2-x}Al$, and Li_9Al_4, are not detected [27]. It should be noted that amorphous $Li_{1+x}Al$ phases may exist but are suggested to be in trace amounts [28]. In contrast, for the back side of the electrode, the characteristic peaks of fcc Al are dominant. Overall, these results confirm that the pristine aluminum foil is partly prelithiated to form a bilayer structure with β-LiAl grown on a single side of the Al foil.

The EIS tests were done for the samples with thinner (P-Al-10, P-Al-20), and with thicker β-LiAl layers (P-Al-90 and P-Al-100). The obtained Nyquist plots are shown in Fig. 2c, in which the high-frequency impedance (>1 kHz, blue zone) is considered as the total contribution of contact resistance (CR), solid electrolyte interface (SEI) and ohmic resistance (OR) [29]. Although some variations in the total impedance of CR, SEI, and OR are observed with the increasing thickness of the β-LiAl

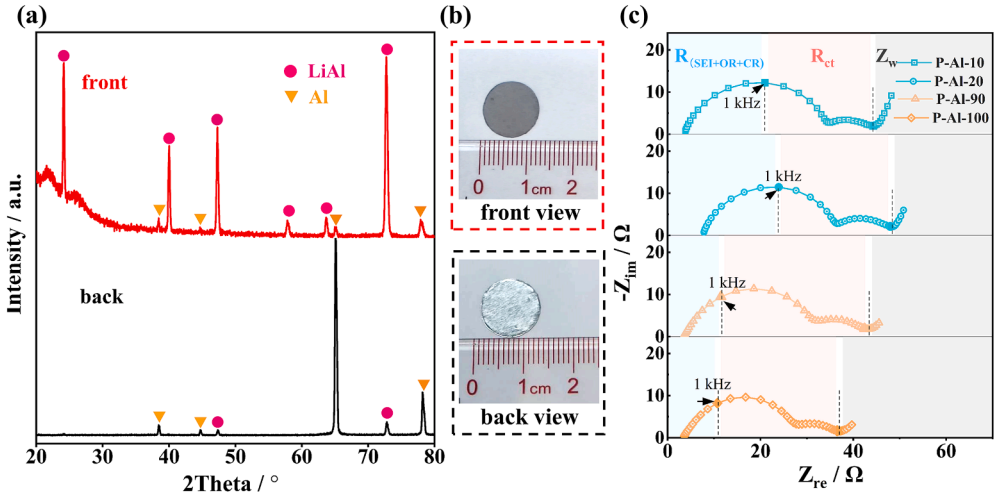

Fig. 2. (a) X-ray diffractograms of (red line: frontside; black line: backside), and (b) photographic images of the front side and back side of P-Al-100. (c) Comparison of EIS Nyquist plots among P-Al-10, P-Al-20, P-Al-90, and P-Al-100 electrodes. The high-frequency impedance (>1kHz) origin from the contact resistance (CR), ohmic resistance (OR), and SEI resistance while the impedance in mid-frequency regime is associated with the charge transfer, and the impedance at low-frequency may be due to the lithium diffusion in the electrode.

layer, we consider the changes minor and are likely a result of the errors from individual cell. This is then confirmed by the EIS spectra obtained from a scratched β-LiAl(Al) electrode (Fig. S2), in which the total impedance increases significantly, and the Nyquist plot is completely changed. This supports that the electrode surface likely remains unperturbed when the β-LiAl layer is growing thicker. Any crack formation and/or secondary SEI formation during lithiation should have been reflected by significant variations in the Nyquist plots.

3.2. Galvanostatic charge-discharge (GCD)

The GCD sequence tests allow us to systematically investigate how Li transports in the β-LiAl layer with various thicknesses, i.e., nominal prelithiation depth varies from 10 to 100 μm. Before presenting the results, it is worth mentioning that the C-rates in these experiments have been defined and summarized in Table S1 since a specific C-rate refers to different currents for different β-LiAl(Al) electrodes due to different prelithiation depths. At the lower C-rate regime (<1.5 C, Fig. 3), the areal capacity of the β-LiAl(Al) electrodes increases almost linearly from approximately 0.085 mAh·cm^{-2} to 0.72 mAh·cm^{-2} as the nominal

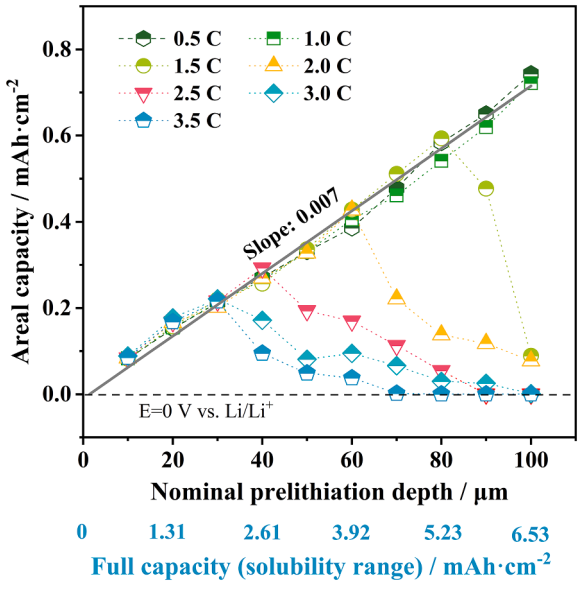

Fig. 3. Areal capacities contributed by the β-LiAl solubility range collected from GCD experiments as a function of pre-lithiation depths (10–100 μm) at various C-rates.

prelithiation depth climbs from 10 to 100 μm. At the higher C-rate regime (≥1.5 C), however, the seemly linear relationship of the prelithiation depth vs. areal capacity no longer remains within the chosen prelithiation range. In general, the thinner the β-LiAl layer, the higher the C-rate can be handled by the β-LiAl(Al) electrode. A complete dataset that covers the C-rate from 0.5 C to 6.1 C is provided in Fig. S3.

It is also important to note that the critical prelithiation depths where the data loses its linearities against areal capacities should be of extra interest. For instance, when the (de-)lithiation rate goes up from 0.5 C to 1.4 C (-8.16 mA·cm^{-2}) in the case of P-Al-90, the areal capacity all maintains at stable values of about 0.66 mAh·cm^{-2} with negligible variation while it dramatically fades at 1.5 C. This critical point implies that the critical C-rate for P-Al-90 is somewhere at 1.4 C (although minor errors could exist among cells). Accordingly, the critical C-rates extrapolated from P-Al-80, P-Al-70, P-Al-60, P-Al-50, P-Al-40, P-Al-30, and P-Al-20 are 1.7 C (-8.81 mA·cm^{-2}), 1.9 C (-8.62 mA·cm^{-2}), 2.1 C (-8.16 mA·cm^{-2}), 2.4 C (-7.77 mA·cm^{-2}), 2.9 C (-7.51 mA·cm^{-2}), 3.5 C (-6.80 mA·cm^{-2}) and 6.0 C (-7.77 mA·cm^{-2}), respectively, which will be discussed later.

Noteworthy, it is contended that the role of SEI formation during the GCD sequence should be minor for two reasons. Firstly, a potential hold of 2 h at 400 mV vs. Li/Li$^+$ is done prior to prelithiation, such that the SEI formation at a higher potential regime is suppressed, similar to what Miao et al. have done [30]. Secondly, the insignificant changes in cell impedance from the EIS results further verify the minor role of SEI in the GCD tests (a significant change in EIS is defined in Fig. S2).

3.3. Galvanostatic intermittent titration technique (GITT)

GITT is a well-established method for extracting information regarding ion diffusion in electrochemical systems, e.g., Li diffusion in this work. Fig. 4a shows a complete GITT set of P-Al-100 during the 1st delithiation process at 0.02 C. During the whole measurement, the phase boundary (α/β) motion is expected to be minimal due to the restricted potential window. When no phase transitions are occurring, the extraction of Li from the β-LiAl shifts the electrode potential towards a more positive level, but not beyond 0.41 V vs. Li/Li$^+$, at which the α and the β phase coexist (delithiation). This single β-LiAl solid solution is also verified by the monotonical relationship of electrode potential as a function of Li content (Fig. 4b). Furthermore, a single titration is enlarged in Fig. 4c, elaborating how to extract ΔE_τ and ΔE_s for diffusivity calculations. Fig. 4d shows that the potential change exhibits a strong linear relation against the square root of the time constant, τ, which implies that our designated measurement meets the assumption of GITT theory. Consequently, the Li diffusivities in β-LiAl can be reasonably

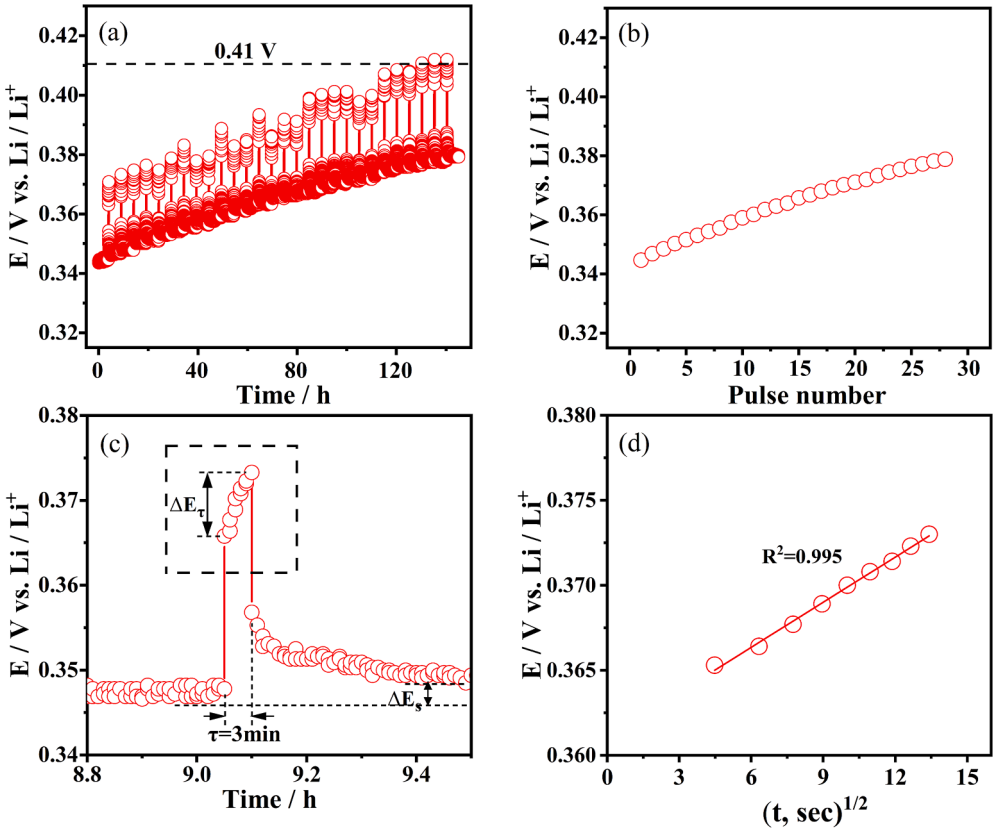

Fig. 4. GITT test for P-Al-100 at 0.02 C during delithiation: (a) A complete GITT set with pulse time of 3 min and rest time of 5 h. (b) Equilibrium potentials after each titration during the GITT test. (c) Demonstration of a single titration that changes the electrode potential from 0.3482 V to 0.3494 V vs. Li/Li^+. (d) Potential variation within a single pulse, i.e., dashed rectangle in (c), is plotted against the square root of time, which exhibits a strong linearity.

estimated by Eq. (1) to be in the order of magnitude of -10^{-7} $cm^2 \cdot s^{-1}$.

3.4. Cyclability and rate performance

To assess the rate capability of the β-LiAl(Al) electrode, a commercial LTO is chosen as the cathode for the galvanostatic cycling owing to its high rate capability and superior cycling stability [31]. The configuration of the assembled cell is illustrated in Fig. 5a. The negative electrode shows a bilayer structure which is achieved by partly prelithiating an Al foil: the upper 100 μm of the Al foil is transformed into β-LiAl while the remaining 80 μm acts as the current collector. It is worth noting that the N/P ratio (the capacity ratio of the negative over the positive electrode) here is ca. 5, much higher than that of commercial LIBs (1.1-1.2), which effectively guarantees the β-LiAl(Al) electrode is being cycled within its solubility range when lithium transport in β-LiAl is not rate limiting.

Fig. 5b shows the discharge-charge profiles of the 2nd, 10th, 50th, 100th, and 300th cycle at 1.0 $mA \cdot cm^{-2}$ with a voltage window of 1.05–1.35 V. All the profiles give similar characteristics: slightly sloping lithiation-delithiation plateaus at around 1.15 and 1.25 V, indicating that the β-LiAl(Al) is cycled within its solubility range, i.e., no problematic α/β phase transformations [5]. Otherwise, the plateaus would have been perfectly flat due to the long lithiation-delithiation plateaus of both Al and LTO [32,33]. When the β-LiAl(Al) anode maintains its crystal structure, the cycling stability is anticipated to be superior, as confirmed hereafter.

The rate performance of the LTO//β-LiAl(Al) cell (Fig. 5c) shows that, during the initial 40 cycles, the discharge capacity gradually drops from 1.38 to 1.1 $mAh \cdot cm^{-2}$ with the current density climbing from 1 to 10 $mA \cdot cm^{-2}$. The reversible capacity raises to the initial level, i.e., 1.38 $mAh \cdot cm^{-2}$ as soon as the current density switches back to 1 $mA \cdot cm^{-2}$. Remarkably, after repeating the above rate-capability test nine more times as the total cycle count approaches 400, this trend is generally maintained, except for the faster degradation in capacity at 10 $mA \cdot cm^{-2}$.

Fig. 5d shows the long-term cycling performance of LTO//β-LiAl(Al) cells at a current range between 0.5–2.0 $mA \cdot cm^{-2}$. One can see that the assembled cells survive after 400 cycles with capacity retention ≥95% in all cases. Specifically, at relatively lower current density (i.e., 0.5 and 1.0 $mA \cdot cm^{-2}$), only about 1% and 2% capacity degradation are observed after 400 cycles, corresponding to 0.003% and 0.005% per cycle. Even at 2 $mA \cdot cm^{-2}$, around 95% capacity maintains after 400 cycles, equivalent to 99.987% capacity retention per cycle, which is beyond the basic requirement of cyclic capacity retention (99.96%) for commercial LIBs [34].

4. Discussion

4.1. Li diffusivity in β-LiAl

Based on the results obtained from the GCD sequence experiments, the critical C-rates for utilizing the solubility range of β-LiAl at room temperature are extrapolated and plotted against the nominal prelithiation depth (Fig. 6). This critical C-rate displays a non-linear decrease with the prelithiation depth increasing from 20 μm to 90 μm. For the C-rates below the critical value, the β-LiAl(Al) electrodes are cycled wholly within the material's solubility range. When the C-rates are beyond the critical ones, the potential of the β-LiAl(Al) electrodes would drop instantaneously to trigger the phase boundary (α/β) movement. In this case, the solubility range of β-LiAl can no longer be reflected by the selected potential range, resulting in a minute level of capacity that is contributed by the reaction at the phase front [32]. In short, the dashed line in Fig. 6 could act as the boundary that separates the solubility range and the phase movement, providing guidance for

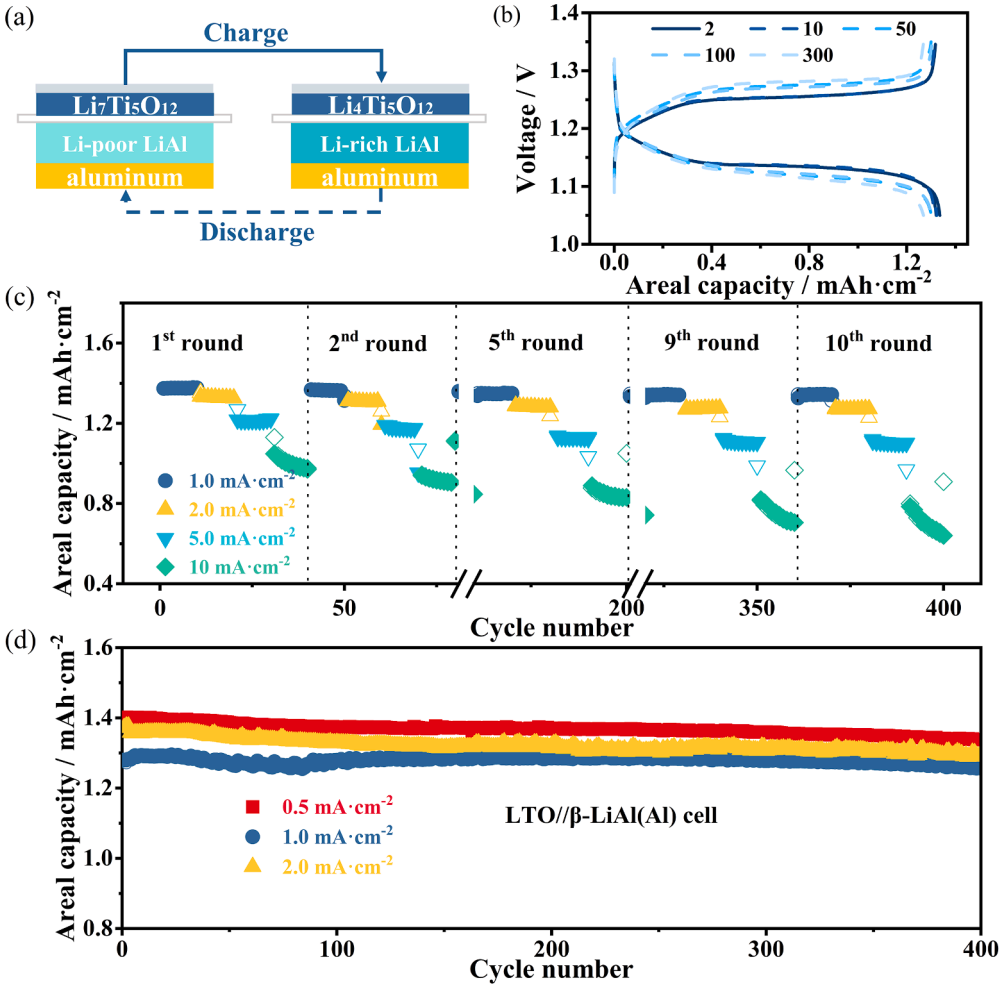

Fig. 5. Electrochemical behaviors of LTO//β-LiAl(Al) cells: (a) A schematic illustration of cell architecture. (b) The galvanostatic charge-discharge profiles during cycling at 1.0 mA·cm^{-2}. (c) The rate performance is evaluated by varying the charge-discharge current between 1.0 and 10 mA·cm^{-2}. (d) The long-term cycling performance at 0.5, 1.0, 2.0 mA·cm^{-2} (details in Table S2).

utilizing the solubility range of the β-LiAl(Al) electrode, and achieving prolonged cycle life. In addition, as the (de-)saturation of the β-LiAl solubility range is governed by lithium diffusion, the Li diffusivity in β-LiAl could be estimated from the critical C-rates presented above. Based on the relationship between diffusion length and diffusivity: $L = \sqrt{2Dt}$ [35], the diffusivity values are calculated to range from 0.28 × 10^{-7} to 5.0 × 10^{-7} cm^2·s^{-1}. This ~10^{-7} diffusion coefficient of Li in β-LiAl is roughly 4 orders of magnitude higher than that in α-Al, which partly explains the high-rate performances of the β-LiAl(Al) electrode (Fig. 5c) when the formation of α-Al is intentionally prevented.

To further investigate the lithium transport in β-LiAl, GITT, a well-known and reliable method, is employed. Fig. 7a and 7b show the lithium diffusivities in P-Al-100 obtained from both the delithiation and the lithiation process. It is observed that the lithium diffusivity during the lithiation tends to decrease noticeably with the increasing content of Li, which agrees well with the previous literature [24]. The higher diffusivity in Li-poor β-LiAl is considered to be associated with more mobile Li vacancies V_{Li} (or less immobile antistructure Li_{Al} in V_{Li}) through which the lithium can transport more freely across the electrode [19,22]. Despite the noticeable variations in the diffusivity values in both cases, it should be noted that all the Li diffusivity values (D_{Li}) are in the same order of magnitude, suggesting that Li atoms exhibit similar kinetic behaviors in the host matrix, i.e., β-LiAl, regardless of extraction/insertion. Moreover, the diffusivities do not seem to vary significantly under different delithiation rates (Fig. S4). Fig. 7c shows that the average D_{Li} at 0.01, 0.02, and 0.04 C generally fall into the same order of magnitude at 10^{-7} cm^2·s^{-1} within the Li content of 47.8–48.2 at%, which are in good agreement with the previously reported values [22]. In addition to the data collected from various C-rates, the D_{Li} is also extracted from the β-LiAl(Al) electrodes with different prelithiation depths. Fig. 7d compares the average D_{Li} in P-Al-60, P-Al-80, and P-Al-100 measured at a fixed C-rate (0.02 C, details in Fig. S5). It turned out to be that the diffusivities are all similar at 10^{-7} cm^2·s^{-1}, with -2.5 × 10^{-7} cm^2·s^{-1} in P-Al-60, -3.6 × 10^{-7} cm^2·s^{-1} in P-Al-80, and -2.7 × 10^{-7} cm^2·s^{-1} in P-Al-100.

To evaluate the data reliability, comparisons of Li diffusivities derived from the GITT experiments were made to the previous reports (Fig. 8). For instance, the measured diffusivities by nuclear magnetic resonance (NMR) were also in the order of 10^{-7} cm^2·s^{-1} at room temperature [22]. As for the GITT methods, only the data at elevated temperatures are available, e.g., at 415 °C [23]. Therefore, the Arrhenius equation $\tilde{D} = \tilde{D}_0 \exp(-\Delta\tilde{H}/RT)$ was used to extrapolate the Li diffusivities at room temperature, also giving similar values of -2 × 10^{-7} cm^2·s^{-1} [23] and -0.9 × 10^{-7} cm^2·s^{-1} [36]. Furthermore, Baranski et al. employed the potentiostatic method and achieved a slightly lower Li diffusivity of -7.7 × 10^{-8} cm^2·s^{-1} at 48 at% Li [37]. On the other hand, Kumagai et al. [38] reported lithium diffusivities in the order of 10^{-10} cm^2·s^{-1} with a Li content of 48–51 at%, which is two orders of magnitude lower than those in this work. The discrepancy may be associated with the difference in electrode structure as well as measurement

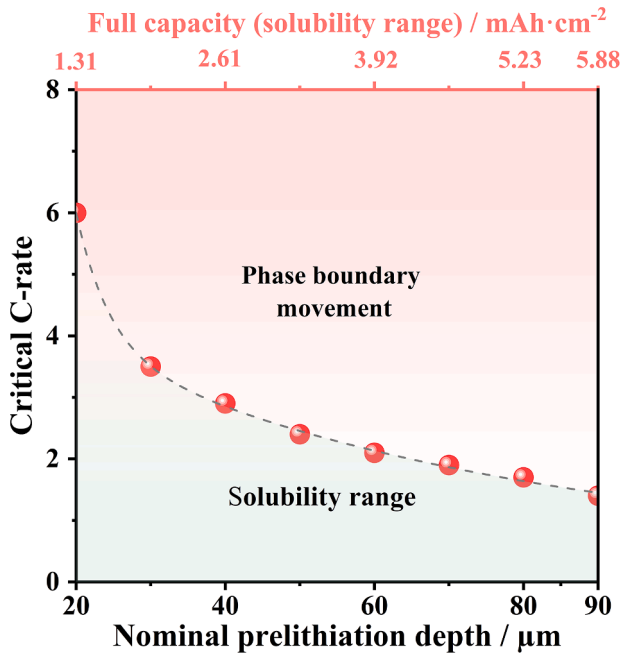

Fig. 6. The critical C-rates (red dot) of the β-LiAl(Al) electrodes at room temperature. The values are obtained from the GCD sequence experiments (details regarding critical C-rate are available in Table S1).

techniques. Generally, the diffusivities presented in this work are reliable, given the self-consistency in the results from GCD and GITT and the consistency with the previously reported data.

4.2. *Rate capability and cycling performance of the β-LiAl(Al) electrode*

From the results in Section 3.2 and the discussion in Section 4.1, the β-LiAl(Al) electrode does exhibit some high rate characteristics considering commercial application demands (1 C = 2 mA·cm^{-2}, single-side) [39]. Therefore, the β-LiAl(Al) electrodes that have similar capacities are selected as the examples here. P-Al-40 can function well at a C-rate as high as 2.9 C, equivalent to an areal current of -7.5 mA·cm^{-2}, which is justified by Li Hong as the true rate performance [39]. It should be noted that the C-rate of 2.9 C is already approaching some of the capacitive devices [40–42].

To explore the limit of the rate capability and evaluate how stable the cycling performance would be, the β-LiAl(Al) electrode with different prelithiation depths is paired against LTO for the cycling tests. The results of capacity retention versus cycle number (Fig. 9) show that, in general, all the β-LiAl(Al) electrodes exhibit a certain resistance to degradation as long as the prelithiation depth is larger than 40 μm, regardless of the (dis-)charging current. More specifically, the P-Al-100 exhibits a cycle life of 500 cycles with a capacity retention of -68% and coulombic efficiency of -98% (Fig. S6) even at 10 mA·cm^{-2}. Interestingly, the cycling performance can be significantly improved by slowing down the (dis-)charging current, giving -83.3, -90.4, and -91.8% capacity retention at 2 mA·cm^{-2}, 1 mA·cm^{-2}, and 0.5 mA·cm^{-2}, respectively. The superior rate capability and decent cycling behaviors of β-LiAl(Al) electrodes are partly supported by our previous GCD results and the GITT analysis. From the application standpoint, the features discussed in this section can make the β-LiAl(Al) electrodes extra suitable for fast-charging Li-ion devices.

On top of the fast-charging capability originating from the fast Li diffusivity, decent cycling performance is achieved by circumventing the huge electrode strain. When the β-LiAl is cycled within the solubility range, namely, the Li storage is considered a single-phase intercalation

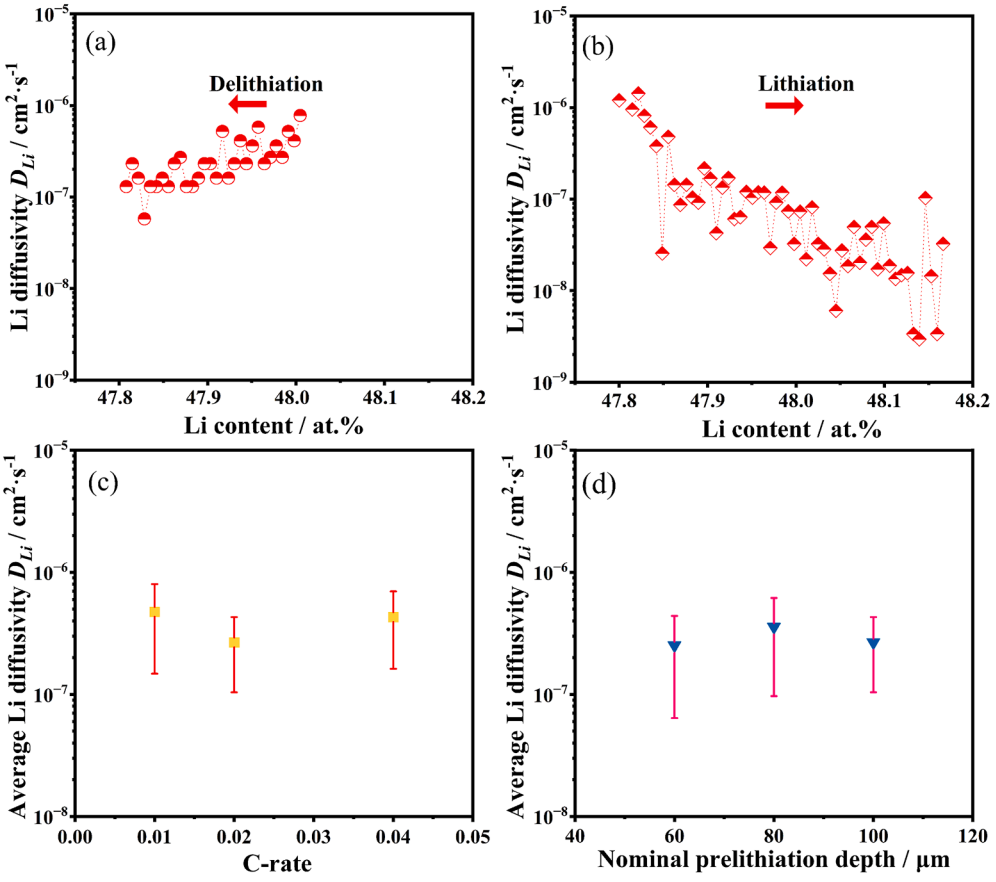

Fig. 7. Li transport kinetics in β-LiAl derived from GITT results. The lithium diffusivity in β-LiAl as a function of Li content at 0.02 C (0.13 mA·cm^{-2}) for delithiation (a) and lithiation (b) process. (c) Average D_{Li} (yellow squares) measured at various delithiation C-rates (0.01 C, 0.02 C and 0.04 C), but from a fixed thickness of β-LiAl layer (P-Al-100). (d) Average D_{Li} (blue triangles) measured at a fixed delithiation C-rate (0.02 C), but from various thicknesses of β-LiAl layers (P-Al-60, P-Al-80, and P-Al-100). The error bars indicate the standard derivation.

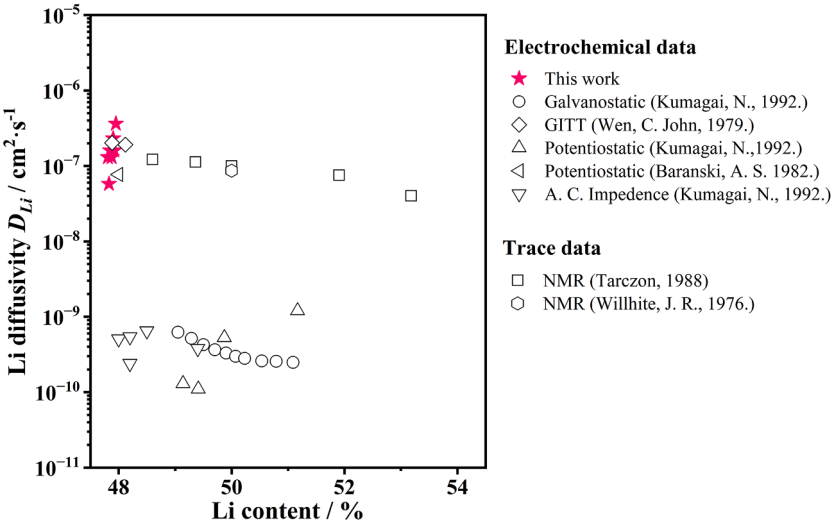

Fig. 8. Comparison of Li diffusivities in β-LiAl in this work with the previously reported values at room temperature.

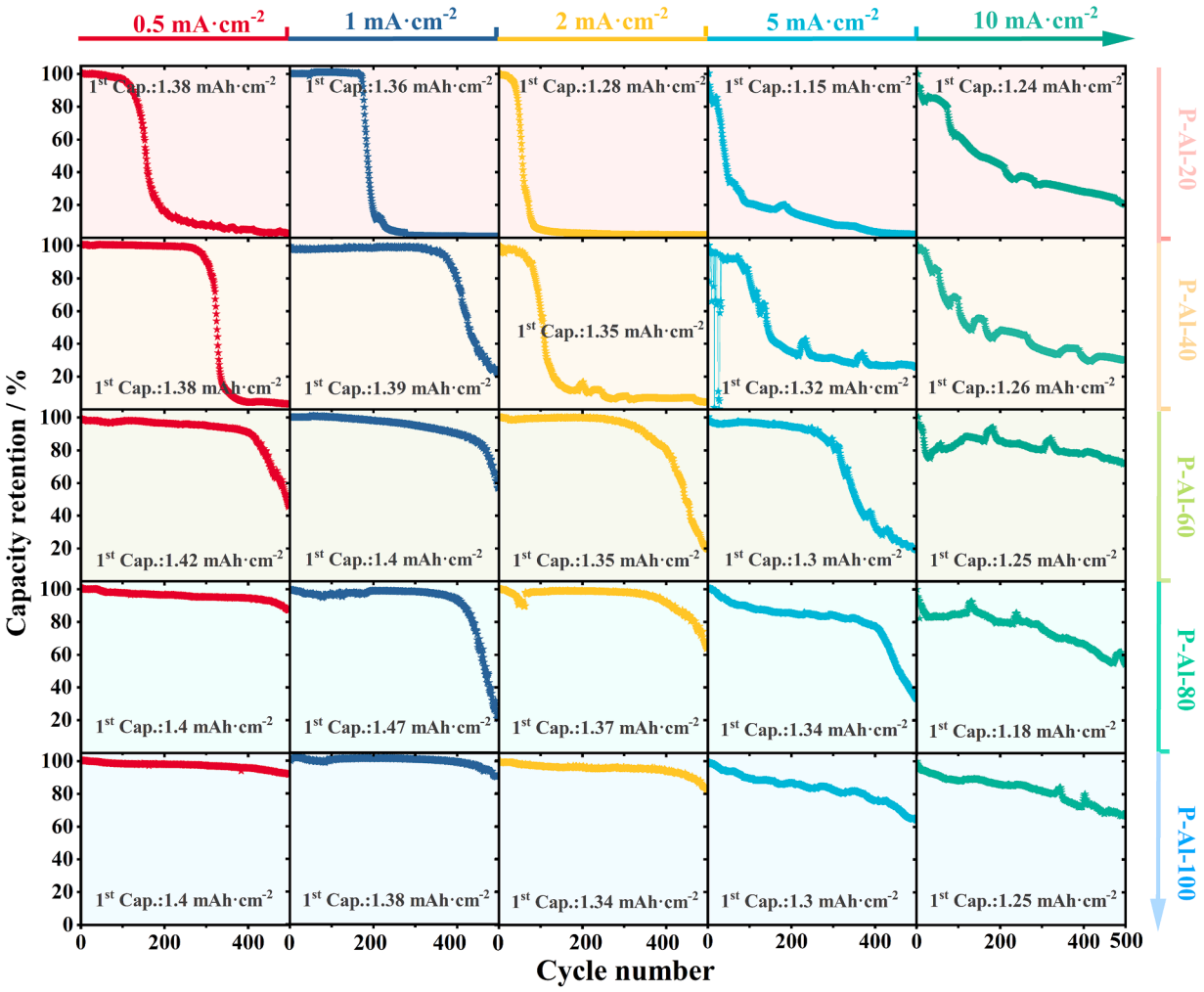

Fig. 9. Plots of capacity retention versus cycle number for the LTO//β-LiAl(Al) cells at different current densities. Five prelithiation depths of β-LiAl(Al) electrodes are presented. It should be noted that '1st cap.' is the abbreviation of the areal capacity of the 1st cycle.

process, no phase transition (and thus significant volume change) is involved. The volume difference of β-LiAl upon (de-)saturation is merely ca. 1.4%, way smaller than the one between α and β, i.e., -95% [5].

4.3. *Kinetic limitations of the β-LiAl(Al) electrode*

Although superior electronic and ionic conductivities endow β-LiAl

the great rate capability [19], the dense structure of thick foils may give rise to kinetic issues, if for example, Li is extracted in an inhomogeneous manner. Different from composite electrodes that have high specific surface areas, our β-LiAl(Al) electrode only offers its projected area (disk size) for the lithium insertion with little surface topography, perhaps imposing negative effects on the rate capability. Therefore, a compromise between the prelithiation depth, i.e., the β-LiAl(Al) thickness, and the charging rate should always exist, as it is bounded by Li diffusivity.

On one hand, the periods recorded from saturating the β-LiAl layers with different thicknesses are extracted from the GCD results (hollow dot and dashed line in Fig. 10a), i.e., the time during which the electrode potential drops from 0.405 V until the α to β phase transformation occurs (determined by the slope at ②/③ in Fig. 1d). These data are termed 'saturation time' hereafter. On the other hand, in order to determine the best rate conditions for the β-LiAl(Al) electrodes with various prelithiation depths, we have also defined three regimes in Fig. 10b based on the data collected from GITT, indicative of three types of phase boundary motions: minimized (zone I), restricted (zone II), and evident (zone III) phase boundary movements. The red solid line represents the minimum time required for Li to spontaneously diffuse through a given thickness of the β-LiAl layer. The values are calculated from the GITT results by using the equation: $L = \sqrt{2Dt}$ when a simple one-dimension diffusion model is assumed [35].

As can be seen, these two datasets generally agree with each other: when the β-LiAl layer is too thick (bold hollow dots in Fig. 10a), a fixed C-rate is corresponding to a significantly large current that can bring down the electrode potential almost instantaneously. As a result, Li insertion tends to move the phase boundary (growth of more β-LiAl) rather than saturating the existing β phase (solubility range), resulting in a dramatic drop in the saturation time, and thus low capacities (zone III). The red solid line in Fig. 10b also segregates this zone from the other two where the β-LiAl(Al) electrodes exhibit a prolonged cycling performance. More specifically, the β-LiAl(Al) electrodes that fall into zone I can theoretically be cycled indefinitely but with relatively low areal capacities, while zone II helps the electrodes to deliver higher capacities though cycling performances may be affected.

By defining these three zones, one should be able to select the appropriate cycling conditions for the β-LiAl(Al) electrodes per their needs. All the data points near the borders among these three zones are bolded. For the prelithiation depth of 80 μm (P-Al-80), the bold hollow circle that is located at the zone II/III border in Fig. 10a implies that the rate limitation might be around 1.5 C (-7.77 mA·cm^{-2}). The same analyses are done for P-Al-60 (hollow triangle), P-Al-50 (inverted hollow triangle), and P-Al-40 (hollow square), with the rate limitations of 2.0 C (-7.77 mA·cm^{-2}), 2.5 C (-8.10 mA·cm^{-2}), and 3.0 C (-7.77 mA·cm^{-2}), respectively. These outcomes are consistent with the analysis of critical C-rates discussed in Section 4.1. Regardless of the kinetic limitations, the β-LiAl(Al) electrodes can already be cycled at rates higher than 1.5 C, exhibiting application potentials in fast-charging devices.

4.4. A comprehensive guide for utilizing the β-LiAl(Al) electrode

The nature of a C-rate is inherently a convolution between capacity and current density, but for the case of β-LiAl(Al) electrodes, the thickness of β-LiAl is related to capacity, $\delta_{\beta-LiAl} \propto C_{\beta-LiAl}$. Therefore, determining a critical C-rate will always be a function of layer thickness and current density. To simplify the situation and provide comprehensive guidance for utilizing the β-LiAl(Al) electrodes across various Li-ion devices, the cyclabilities of various electrode thicknesses at different current densities (0.5–10 mA·cm^{-2}) are mapped out. The cycle number of each electrode is extracted until an 80% capacity retention. As anticipated, it is observed from Fig. 11a that the cycle life of the β-LiAl (Al) electrode exhibits correlations with the prelithiation depth and the current density. Within the testing range in this study, a general trend is observed: a higher prelithiation depth and/or a lower C-rate would give a longer cycle life to the β-LiAl(Al) electrode. For example, the β-LiAl(Al) electrode with a prelithiation depth of 100 μm can be cycled 500 times at 0.5 or 1 mA·cm^{-2} or more than 300 times at 2, 5, or 10 mA·cm^{-2}, while maintaining >90% or >80% of the initial capacities, respectively. On the other hand, the β-LiAl(Al) electrode with a thinner nominal prelithiation depth of 20 μm gives a worse performance of fewer than 200 cycles at all rates. The commercial LIBs are required to tolerate a charging rate of 1.5 C, corresponding to -2.25–3 mA·cm^{-2} (considering the cell areal capacity of 1.5–2 mAh·cm^{-2}), illustrated as horizontal lines in Fig. 11a. It can be seen that even at 1.5 C (i.e., 2.25–3 mA·cm^{-2}), the β-LiAl(Al) electrode can still give a lifetime of over 300 when the prelithiation depth is over 60 μm.

To summarize, the mapping offers an overview of the cycle behaviors under various conditions, providing a general guideline for the practical use of the β-LiAl(Al) electrodes. For instance, if a Li-ion cell is required to be charged at an extremely fast rate (e.g., > 5 mA·cm^{-2}), the user should consider using the β-LiAl(Al) electrode with a prelithiation depth over 60 μm, e.g., 100 μm. At a moderate charging rate (e.g., 2–5 mA·cm^{-2}), the β-LiAl(Al) electrode with the prelithiation depth of 40–60 μm may be sufficient, such that a thinner electrode can be made. Lastly, when the charging rate is not the main concern, a lower one would always be beneficial.

To evaluate the β-LiAl electrode across all dimensions, the performance indicators (e.g., volumetric capacity, charging rate, cycle life) of the LTO//β-LiAl(Al) cells are compared to those of supercapacitors [41, 44–46] and Li-ion batteries with typical anodes (e.g., LTO [47], Si [48–50], Li [51], TiO_2 [52]) reported in the literature (Fig. 11b).

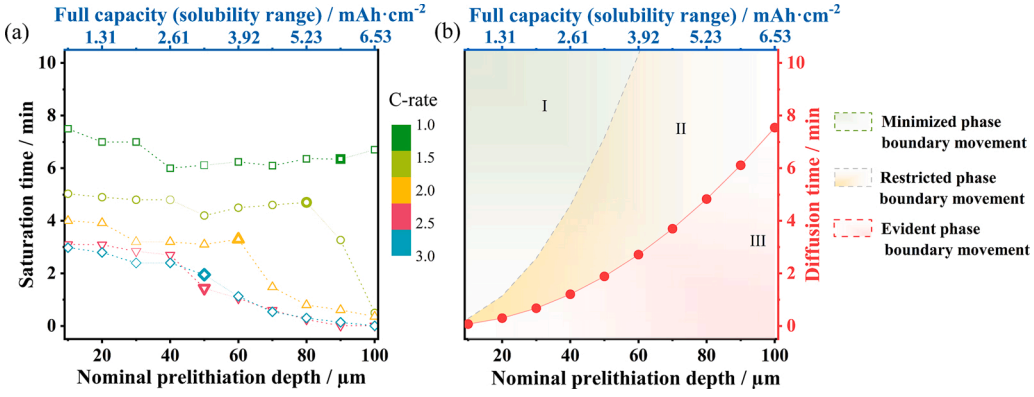

Fig. 10. Kinetic limitation for β-LiAl (Al) electrodes: (a) The saturation time at various C-rates (hollow dots) were collected from the GCD results. (b) The calculated diffusion time (red solid dot-line) is obtained from the GITT results. For a planar (e.g., a foil) electrode, which is assumed to follow a one-dimension diffusion model [35], the diffusion depth should be proportional to the square root of time: $L = \sqrt{2Dt}$. As for the β-LiAl(Al) electrode working within its solubility range, the diffusion depth L is limited to the β-LiAl layer thickness, ranging from 19.5 to 195 μm considering 95% lattice volume difference [6]. Hence the time required for diffusing through the β-LiAl layer is calculated by the rearranged equation: $t = L^2/2D$.

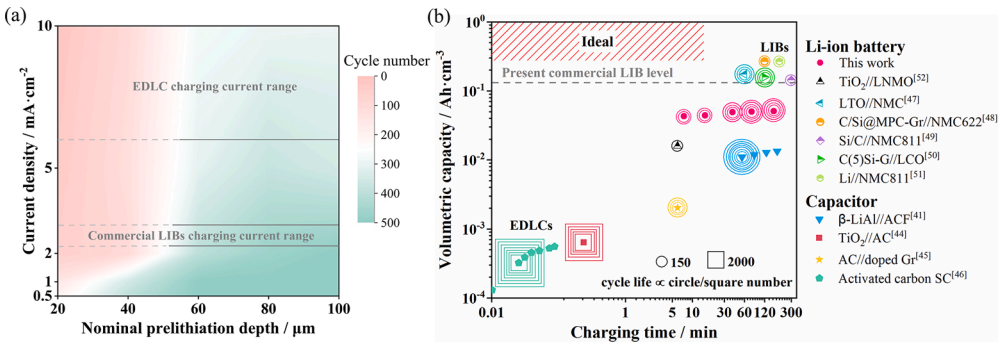

Fig. 11. (a) Mapping of cycle life for LTO//β-LiAl(Al) cells prior to ≥80% capacity retention at different current densities. The horizontal lines indicate the common charging current densities for commercial EDLCs and LIBs, considering cell areal capacity of 1.5–2 mAh·cm^{-2} (single-side) [39] and the common charging C-rate of 1.5 C. (b) Comparisons of our LTO//β-LiAl(Al) cell with some previously reported Li-ion full cells and EDLCs. The volumetric capacity is normalized to the stack volume (cathode, anode, current collectors, and separator) while the dashed line generally represents the commercial standard for LIBs, which is calculated from an energy density of 0.5 Wh·cm^{-3} (normalized to the package volume) [43]. The red shaded zone (upper left) indicates the ideal volumetric capacity for rechargeable batteries: over 0.243 Ah·cm^{-3} (package volumetric energy > 800 Wh·L^{-1}, given the mid-point voltage of 3.3 V for commercial LFP//graphite LIBs) by charging within 15 min [29,43], and a cycle life more than 5000. The rectangular and circular rings that surround the data points quantitatively describe the cyclability of the devices.

Volumetric capacities instead of gravimetric ones are chosen for comparisons since Y. Gogotsi and P. Simon pointed out that the latter may not reflect the true performances due to the extremely low densities of some materials and/or the omittance of the electrolyte weight [53]. It should be noted that the volumetric capacities here are normalized to the volume of the stack, namely, cathode, anode, current collectors, and separator (detailed parameters for LTO// β-LiAl(Al) cells are available in Table S3). As shown in Fig. 11b, the LTO//β-LiAl(Al) cell stands between electrical double-layer capacitors (EDLCs) and Li-ion batteries, delivering a capacity of -0.05 Ah·cm^{-3}. Despite the lower capacity than the state-of-art LIBs, our cells exhibit a superior fast-charging capability: they can be charged within 15 min and last for ≥300 cycles. Moreover, the superiority of the LTO//β-LiAl(Al) cell is also highlighted by competing with the activated carbon (AC)//doped graphite (Gr) Li-ion capacitor [45]. Our cell delivers a higher volumetric capacity (nearly 20 times in magnitude than AC//doped Gr capacitor) by charging below 10 min and achieves a comparable cycle life simultaneously.

Considering the energy density of Li-ion cells, LTO may not be an appropriate anode candidate due to its high plateau potential of -1.5 V vs. Li/Li$^+$, which limits the voltage window, and thereby the cell energy. Consequently, the NMC811 cathode (NEI corporation) with an areal capacity of -2 mAh·cm^{-2} and thickness of 60 μm is assumed to pair against the β-LiAl(Al) vs. the graphite. The calculated volumetric energy densities are provided in Table S4-S5. As can be seen, the energy density of the NMC811//β-LiAl(Al) cell is not advantageous, as compared to the NMC811//graphite cell, but it has been highlighted multiple times that ideal anodes in LIBs should be expected to balance the cost, capacity, and manufacturing complexity for every application. The successful commercialization of LTO anodes in the last century can be a good example in this regard. Overall, the combined performance characteristics of LIBs and EDLCs pave the way for β-LiAl in fast-charging applications in energy storage devices, especially taking into account the simple preparation of foil, low cost (avoiding the use of Cu), and lower likelihood of Li dendrite formation. It is believed that the simplified electrode design could eliminate the labor- and energy-intensive steps, such as mixing, pasting, and baking, and thereby better realizing sustainability [41].

5. Conclusions and implementation concerns

In summary, the charging behaviors and cycling performances of the β-LiAl(Al) electrodes are systematically studied in this work, providing insights into Li transport characteristics in the β-LiAl system. The Li diffusivity in the β-LiAl is determined to be in an order of 10^{-7} cm^2·s^{-1} at room temperature. Accordingly, the maximum charging current of the electrodes can be projected depending on their thicknesses. For instance, the P-Al-80 electrode can tolerate a charge-discharge current as high as ca. 8.8 mA·cm^{-2} while giving acceptable cycling lives (> 80% capacity retention after 360 cycles for 5 mA·cm^{-2} and after 250 cycles for 10 mA·cm^{-2}). Furthermore, the cycle life assessment of the electrodes shows a strong dependence on the prelithiation depth and current density. At lower current densities (< 2.0 mA·cm^{-2}), the electrodes exhibit a great cycling stability of above 80% after 400 cycles with a sufficient prelithiation depth (i.e., ≥ 60 μm) except in one sample. Although this cycling stability seems to be negatively affected by the higher current densities, such as 5 mA·cm^{-2} and 10 mA·cm^{-2}, 80% of the initial capacities are properly maintained after at least 300 cycles. Lastly, the mapping of cyclability at different current densities further guides the utility of the β-LiAl(Al) electrodes.

Looking forward, some may ask about implementing a β-LiAl(Al) anode in a commercial LIB and how this might be processed. Given that the cathode is the limitation for the full cell capacity, the specifications for the anode are then selected to match accordingly (e.g., desired N/P ratio, thickness, etc.). If we have a cathode with -1.25 mAh·cm^{-2}, then this should be paired with a β-LiAl(Al) anode that has a prelithiation layer at least 60 μm-thick in order to have 400 stable cycles at lower rates (≤ 2mA·cm^{-2}) or 300 stable cycles at higher rates (≥ 5 mA·cm^{-2} and ≤ 10 mA·cm^{-2}), per Fig. 11a. Likewise, the prelithiation depth can be extrapolated to pair β-LiAl(Al) anodes with almost any cathodes that have higher/lower capacities, it is simply a matter of selecting the current density and the desired cycle life.

The prelithiation step itself is effectively trivial and can be done either electrochemically (by controlling the electric charge of lithiation) or mechanically (by controlling the weight of Li metal). For example, 10 μm nominal prelithiation depth can be achieved by counting -2.7 mAh·cm^{-2} electric charge during electrochemical lithiation. From a chemical/metallurgical perspective, specifying the Li foil thickness for prelithiation is very convenient as 1 μm of Li foil set on Al will prelithiate -1 μm Al to form β-LiAl. For the case of the 60 μm-thick nominal prelithiated layer, a -60 μm-thick Li foil can be used. To maintain excellent structural integrity and electrical conductivity a 100 μm-thick Al foil could be used as the precursor (i.e., Cathode: -1.25 mAh·cm^{-2} || Anode: 60 μm Li foil + 100 μm Al foil). However, the residual thickness (-40 μm) of Al necessary for maintaining good electrode integrity without affecting cycle life is still an open question to be addressed, although the authors have seen no evidence of trouble with 40% residual Al thickness. Despite the great potential of LiAl(Al) in LIBs, questions about whether the superior electrode characteristics will be maintained at a lower N/P ratio, or what the optimized N/P ratio for best performance is, can be further explored in the future. Nevertheless, it appears that the history of Al anodes in lithium-ion batteries may not be finished just yet, and the challenge remaining is to figure out how to utilize a higher portion of its capacity without sacrificing the electrochemical performances.

CRediT authorship contribution statement

Jia Zhang: Investigation, Visualization, Writing – original draft. **Tianye Zheng:** Methodology, Supervision, Writing – original draft, Writing – review & editing. **Kwok-ho Lam:** Resources, Funding acquisition. **Steven T. Boles:** Conceptualization, Supervision, Project administration, Writing – review & editing.

Declaration of Competing Interest

The authors declare that they have no known competing financial interests or personal relationships that could have appeared to influence the work reported in this paper.

Acknowledgments

J. ZHANG is supported by the Teaching Postgraduate Studentship (TPS) Scheme from Department of Electrical Engineering at The Hong Kong Polytechnic University (PolyU). T. ZHENG would like to acknowledge the "PolyU Distinguished Postdoctoral Fellowship Scheme" (1-YWBT). K. H. LAM acknowledges the financial support from the Hong Kong Polytechnic University and University of Glasgow. S. T. BOLES acknowledges the ENERSENSE research initiative (68024013) at Norwegian University of Science and Technology (NTNU), Norway. The authors are thankful to Toyo Aluminum K.K., Japan, for providing the 180 μm-thick Al foil samples.

Supplementary materials

Supplementary material associated with this article can be found, in the online version, at doi:10.1016/j.electacta.2023.142437.

References

[1] B. Rao, R. Francis, H. Christopher, Lithium-aluminum electrode, J. Electrochem. Soc. 124 (1977) 1490.
[2] J. Wang, I. Raistrick, R.A. Huggins, Behavior of some binary lithium alloys as negative electrodes in organic solvent-based electrolytes, J. Electrochem. Soc. 133 (1986) 457.
[3] G.E. Blomgren, The development and future of lithium ion batteries, J. Electrochem. Soc. 164 (2016) A5019.
[4] B.T. Heligman, A. Manthiram, Elemental foil anodes for lithium-ion batteries, ACS Energy Lett. 6 (2021) 2666–2672.
[5] T. Zheng, D. Kramer, R. Mönig, S.T. Boles, Aluminum foil anodes for li-ion rechargeable batteries: the role of li solubility within β-LiAl, ACS Sustain. Chem. Eng. 10 (2022) 3203–3210.
[6] H. Wang, X. Luo, H. Wang, T. Ma, M. Lv, X. Song, S. Jin, X. Chang, X. Li, The progress on aluminum-based anode materials for lithium-ion batteries, J. Mater. Chem. A 8 (2020) 25649–25662.
[7] T. Zheng, X. Wang, E. Jain, D. Kramer, R. Monig, M. Seita, S.T. Boles, Granular phase transformation of polycrystalline aluminum during electrochemical lithiation, Scr. Mater. 188 (2020) 164–168.
[8] G. Oltean, C.W. Tai, K. Edström, L. Nyholm, On the origin of the capacity fading for aluminium negative electrodes in Li-ion batteries, J. Power Sources 269 (2014) 266–273.
[9] I. Offen-Polak, M. Auinat, N. Sezin, Y. Ein-Eli, M. Balaish, A binary carbon-free aluminum anode for lithium-ion batteries, J. Power Sources 498 (2021), 229902.
[10] T. Zheng, D. Kramer, M.H. Tahmasebi, R. Mönig, S.T. Boles, Exploring the reversibility of phase transformations in aluminum anodes through operando light microscopy and stress analysis, ChemSusChem 13 (2020) 5910–5920.
[11] H. Xu, S. Li, C. Zhang, X. Chen, W. Liu, Y. Zheng, Y. Xie, Y. Huang, J. Li, Roll-to-roll prelithiation of Sn foil anode suppresses gassing and enables stable full-cell cycling of lithium ion batteries, Energy Environ. Sci. 12 (2019) 2991–3000.
[12] C.L. Berhaut, D.Z. Dominguez, D. Tomasi, C. Vincens, C. Haon, Y. Reynier, W. Porcher, N. Boudet, N. Blanc, G.A. Chahine, Prelithiation of silicon/graphite composite anodes: benefits and mechanisms for long-lasting Li-Ion batteries, Energy Stor. Mater. 29 (2020) 190–197.
[13] N. Liu, L. Hu, M.T. McDowell, A. Jackson, Y. Cui, Prelithiated silicon nanowires as an anode for lithium ion batteries, ACS Nano 5 (2011) 6487–6493.
[14] J. Morales, R. Trócoli, S. Franger, J. Santos-Pena, Cycling-induced stress in lithium ion negative electrodes: liAl/$LiFePO_4$ and $Li_4Ti_5O_{12}$/$LiFePO_4$ cells, Electrochim. Acta 55 (2010) 3075–3082.
[15] Y. Yu, S. Li, H. Fan, H. Xu, M. Jiang, Y. Huang, J. Li, Optimal annealing of Al foil anode for prelithiation and full-cell cycling in Li-ion battery: the role of grain boundaries in lithiation/delithiation ductility, Nano Energy 67 (2020), 104274.
[16] P.J. Crowley, K.P. Scanlan, A. Manthiram, Diffusional lithium trapping as a failure mechanism of aluminum foil anodes in lithium-ion batteries, J. Power Sources 546 (2022), 231973.
[17] T. Chen, A.C. Thenuwara, W. Yao, S.E. Sandoval, C. Wang, D.H. Kang, D. Majumdar, R. Gopalaswamy, M.T. McDowell, Benchmarking the degradation behavior of aluminum foil anodes for lithium-ion batteries, Batter. Supercaps (2022), e202200363.
[18] H. Li, T. Yamaguchi, S. Matsumoto, H. Hoshikawa, T. Kumagai, N.L. Okamoto, T. Ichitsubo, Circumventing huge volume strain in alloy anodes of lithium batteries, Nat. Commun. 11 (2020) 1–8.
[19] T. Tokuhiro, S. Susmam, T.O. Brun, K.J. Volin, ^{7}Li NMR relaxation in supreionic β-lithium aluminum, J. Phys. Soc. Jpn 58 (1989) 2553–2569.
[20] T. Brun, J. Jorgensen, M. Misawa, F. Rotella, S. Susman, D. Mildner, Defects and disorder in the fast-ion electrode lithium-aluminum, J. Electrochem. Soc. 129 (1982) 2509.
[21] S. Chen, J.C. Tarczon, W. Halperin, J. Brittain, Li self-diffusion in pure and doped β-LiAl using pulsed-field gradient NMR, J. Phys. Chem. Solids 46 (1985) 895–904.
[22] J. Tarczon, W. Halperin, S. Chen, J. Brittain, Vacancy-antistructure defect interaction diffusion in β-LiAl and β-LiIn, Mater. Sci. Eng. A 101 (1988) 99–108.
[23] C.J. Wen, B. Boukamp, R.A. Huggins, W. Weppner, Thermodynamic and mass transport properties of "LiAl, J. Electrochem. Soc. 126 (1979) 2258.
[24] C. Wen, C. Ho, B. Boukamp, I. Raistrick, W. Weppner, R. Huggins, Use of electrochemical methods to determine chemical-diffusion coefficients in alloys: application to 'LiAl, Int. Met. Rev. 26 (1981) 253–268.
[25] C.J. Wen, W. Weppner, B. Boukamp, R. Huggins, Electrochemical investigtion of solubility and chemical diffusion of lithium in aluminum, Metall. Trans. B 11 (1980) 131–137.
[26] Y. Geronov, P. Zlatilova, G. Staikov, The secondary lithium-aluminium electrode at room temperature. II. Kinetics of the electrochemical formation of the lithium-aluminium alloy, J. Power Sources 12 (1984) 155–165.
[27] T. Zheng, J. Zhang, W. Jin, S.T. Boles, Utilization of Li-Rich Phases in Aluminum Anodes for Improved Cycling Performance through Strategic Thermal Control, ACS Appl. Energy Mater. 6 (2023) 1845–1852.
[28] B. Qin, T. Diemant, H. Zhang, A. Hoefling, R.J. Behm, J. Tübke, A. Varzi, S. Passerini, Revisiting the electrochemical lithiation mechanism of aluminum and the role of Li-rich phases ($Li_{1+x}Al$) on capacity fading, ChemSusChem 12 (2019) 2609–2619.
[29] C.Y. Wang, T. Liu, X.G. Yang, S. Ge, N.V. Stanley, E.S. Rountree, Y. Leng, B. D. McCarthy, Fast charging of energy-dense lithium-ion batteries, Nature 611 (2022) 485–490.
[30] J. Miao, C.V. Thompson, Kinetic study of the initial lithiation of amorphous silicon thin film anodes, J. Electrochem. Soc. 165 (2018) A650.
[31] M.M. Thackeray, K. Amine, $Li_4Ti_5O_{12}$ spinel anodes, Nat. Energy 6 (2021), 683-683.
[32] T. Zheng, D. Kramer, M.H. Tahmasebi, R. Mönig, S.T. Boles, Improvement of the cycling performance of aluminum anodes through operando light microscopy and kinetic analysis, ChemSusChem 13 (2020) 974–985.
[33] H.C. Chiu, X. Lu, J. Zhou, L. Gu, J. Reid, R. Gauvin, K. Zaghib, G.P. Demopoulos, Capacity fade mechanism of $Li_4Ti_5O_{12}$ nanosheet anode, Adv. Energy Mater. 7 (2017), 1601825.
[34] Z. Lin, T. Liu, X. Ai, C. Liang, Aligning academia and industry for unified battery performance metrics, Nat. Commun. 9 (2018) 1–5.
[35] A.J. Bard, L.R. Faulkner, H.S. White, Electrochemical methods: Fundamentals and Applications, John Wiley & Sons, 2022.
[36] J. Willhite, N. Karnezos, P. Cristea, J. Brittain, Li^7 self diffusion in LiAl—an NMR study, J. Phys. Chem. Solids 37 (1976) 1073–1076.
[37] A. Baranski, W. Fawcett, The formation of lithium-aluminum alloys at an aluminum electrode in propylene carbonate, J. Electrochem. Soc. 129 (1982) 901.
[38] N. Kumagai, Y. Kikuchi, K. Tanno, F. Lantelme, M. Chemla, Electrochemical investigation of the diffusion of lithium in β-LiAl alloy at room temperature, J. Appl. Electrochem. 22 (1992) 728–732.
[39] H. Li, Practical evaluation of Li-ion batteries, Joule 3 (2019) 911–914.
[40] B. Li, L. Xie, Y. Liu, D. Yao, L. Yao, L. Deng, $NiCo_2S_4$ nanosheets decorated on nitrogen-doped hollow carbon nanospheres as advanced electrodes for high-performance asymmetric supercapacitors, Nanotechnology 33 (2021), 085404.
[41] T. Zheng, S.T. Boles, Simplifying electrode design for lithium-ion rechargeable cells, ACS Omega 7 (2022) 37867–37872.
[42] T. Zheng, M.H. Tahmasebi, B. Li, Y. Li, S. Ran, T.S. Glen, K.H. Lam, I.S. Choi, S. T. Boles, Sputtered Titanium Nitride Films on Titanium Foam Substrates as Electrodes for High-Power Electrochemical Capacitors, ChemElectroChem 5 (2018) 2199–2207.
[43] G.G. Eshetu, H. Zhang, X. Judez, H. Adenusi, M. Armand, S. Passerini, E. Figgemeier, Production of high-energy Li-ion batteries comprising silicon-containing anodes and insertion-type cathodes, Nat. Commun. 12 (2021) 1–14.
[44] G. Calcagno, A. Lotsari, A. Dang, S. Lindberg, A. Palmqvist, A. Matic, C. Cavallo, Fast charging negative electrodes based on anatase titanium dioxide beads for highly stable Li-ion capacitors, Mater. Today Energy 16 (2020), 100424.
[45] S.R. Sivakkumar, A. Pandolfo, Evaluation of lithium-ion capacitors assembled with pre-lithiated graphite anode and activated carbon cathode, Electrochim. Acta 65 (2012) 280–287.
[46] M.F. El-Kady, V. Strong, S. Dubin, R.B. Kaner, Laser scribing of high-performance and flexible graphene-based electrochemical capacitors, Science 335 (2012) 1326–1330.
[47] H.G. Jung, M.W. Jang, J. Hassoun, Y.K. Sun, B. Scrosati, A high-rate long-life $Li_4Ti_5O_{12}$/Li $[N_{i0.45}Co_{0.1}Mn_{1.45}]$ O_4 lithium-ion battery, Nat. Commun. 2 (2011) 1–5.

[48] Y. Son, N. Kim, T. Lee, Y. Lee, J. Ma, S. Chae, J. Sung, H. Cha, Y. Yoo, J. Cho, Calendering-compatible macroporous architecture for silicon-graphite composite toward high-energy lithium-ion batteries, Adv. Mater. 32 (2020), 2003286.
[49] J.Y. Li, G. Li, J. Zhang, Y.X. Yin, F.S. Yue, Q. Xu, Y.G. Guo, Rational design of robust Si/C microspheres for high-tap-density anode materials, ACS Appl. Mater. Interface 11 (2019) 4057–4064.
[50] J. Sung, N. Kim, J. Ma, J.H. Lee, S.H. Joo, T. Lee, S. Chae, M. Yoon, Y. Lee, J. Hwang, Subnano-sized silicon anode via crystal growth inhibition mechanism and its application in a prototype battery pack, Nat. Energy 6 (2021) 1164–1175.
[51] X. Ren, L. Zou, X. Cao, M.H. Engelhard, W. Liu, S.D. Burton, H. Lee, C. Niu, B. E. Matthews, Z. Zhu, Enabling high-voltage lithium-metal batteries under practical conditions, Joule 3 (2019) 1662–1676.
[52] M. Agostini, S. Brutti, M. Navarra, S. Panero, P. Reale, A. Matic, B. Scrosati, A high-power and fast charging Li-ion battery with outstanding cycle-life, Sci. Rep. 7 (2017) 1–7.
[53] Y. Gogotsi, P. Simon, True performance metrics in electrochemical energy storage, Science 334 (2011) 917–918.